OUKA
The University of Osaka
Institutional Knowledge Archive

Title	Enhancing Joint Performance of Dissimilar A6061 Aluminum and Galvanized Steel Using Dual-Beam Laser Brazing
Author(s)	Ogura, Tomo; Wakazono, Reiko; Yamashita, Shotaro et al.
Citation	Journal of Materials Engineering and Performance. 2026
Version Type	VoR
URL	https://hdl.handle.net/11094/106867
rights	This article is licensed under a Creative Commons Attribution 4.0 International License.
Note	

The University of Osaka Institutional Knowledge Archive : OUKA

https://ir.library.osaka-u.ac.jp/

The University of Osaka

JMEPEG
https://doi.org/10.1007/s11665-026-14716-y

©The Author(s)
1059-9495/$19.00

ORIGINAL RESEARCH ARTICLE

Enhancing Joint Performance of Dissimilar A6061 Aluminum and Galvanized Steel Using Dual-Beam Laser Brazing

Tomo Ogura, Reiko Wakazono, Shotaro Yamashita, and Kazuyoshi Saida

Submitted: 27 March 2026 / Revised: 11 June 2026 / Accepted: 7 July 2026

A dual-beam laser brazing process was investigated to improve joint performance in dissimilar joining of A6061 aluminum alloy and GA steel. In this approach, a preheating beam was applied to control the interfacial condition prior to brazing, followed by a main laser beam for filler metal melting. Microstructural observations and tensile shear tests revealed that the dual-beam configuration suppressed blowhole formation and significantly enhanced wettability, leading to improved joint strength. Under the optimum condition (preheating: 200 W, main: 1.5 kW), base metal fracture occurred in both A6061/SPCC-GA and A6061/980DP-GA joints, demonstrating the superior performance of the dual-beam process. Numerical simulations were conducted to elucidate the underlying mechanisms, showing that increasing laser power increases the wetting width and decreases the bead wetting angle. Improved wettability in the dual-beam process was attributed to the elevated SPCC-GA interface temperature prior to filler metal spreading, which promotes melting of the galvanized coating and reduces interfacial resistance. These findings demonstrate that controlling the interfacial thermal condition via a dual-beam configuration is an effective strategy to enhance wettability and joint performance in dissimilar laser brazing.

Keywords laser brazing, dissimilar joining, aluminum alloy, galvanized steel, wettability, interfacial reaction

1. Introduction

Improving fuel efficiency has become a critical issue in the automotive industry, driving extensive efforts toward vehicle lightweighting through the application of aluminum alloys and multi-material structures (Ref 1, 2). Aluminum alloys exhibit high specific strength, excellent corrosion resistance, and good recyclability. However, their relatively high cost and inferior weldability compared with steels make the complete replacement of steel components impractical. Consequently, reliable dissimilar joining technologies between aluminum alloys and steels are essential for lightweight vehicle body structures (Ref 3, 4). Conventional fusion welding between aluminum alloys and steels is difficult because brittle Fe-Al intermetallic compounds (IMCs) readily form at the interface, significantly deteriorating joint performance (Ref 3, 5). To overcome this issue, alternative joining techniques such as solid-state joining and brazing have attracted considerable attention (Ref 6-9). Among these techniques, laser brazing is particularly attractive because of its localized heat input, high processing speed, and excellent controllability, and it has already been partially implemented in automotive manufacturing (Ref 10-12).

In automotive structures, coated steels such as galvanized (GI) and galvannealed (GA) steels are widely used because of their superior corrosion resistance (Ref 13, 14). Therefore, reliable joining between aluminum alloys and coated steels is increasingly important for multi-material structures (Ref 15-18). However, laser brazing of aluminum alloys to GA steel is more difficult than that to GI steel because the Fe-Zn intermetallic compounds in the GA coating exhibit relatively high melting temperatures. Consequently, higher heat input is required to melt the coating layer, which promotes excessive interfacial reactions, Zn vaporization, and formation of brittle Fe-Al IMCs. In a conventional single-beam process, increasing the heat input improves wettability but simultaneously promotes porosity formation caused by Zn vaporization. Conversely, reducing the heat input suppresses porosity but deteriorates wetting and spreading behavior. Therefore, precise control of the interfacial thermal condition is essential.

In our previous study, dissimilar laser brazing between aluminum alloys and GA steel was successfully achieved using optimized process conditions and an interlayer (Ref 19). Furthermore, in our previous numerical study, the thickness distribution of IMCs at the joint interface was predicted for both single-beam and dual-beam laser brazing using a coupled numerical approach (Ref 20). The results demonstrated that the

This article is an invited paper selected from abstracts submitted to the 6th International Conference on Nanojoining and Microjoining (NMJ 2025), held from November 17–21, 2025, in Yeongju, South Korea. It has been expanded from the original presentation. The issue was organized by Anming Hu, University of Tennessee Knoxville; Jeongwon Yoon, Chungbuk National University; Jolanta Janczak-Rusch, EMPA; Guisheng Zou, Tsinghua University; Tomokazu Sano, University of Osaka; Susann Hausner, TU Chemnitz; and Hyun-sik Kim, University of Seoul.

Tomo Ogura, Reiko Wakazono, Shotaro Yamashita, and **Kazuyoshi Saida**, Division of Materials and Manufacturing Science, Graduate School of Engineering, The University of Osaka, Osaka, Japan. Contact e-mail: tomo.ogura@mapse.eng.osaka-u.ac.jp.

Published online: 12 August 2026

dual-beam configuration improved thermal distribution control and enabled better control of IMC formation and bead geometry compared with the conventional single-beam process. To overcome this trade-off, a dual-beam laser brazing process is considered in the present study. In this approach, one laser beam is used for preheating to melt the GA coating layer, while the second beam is employed for the brazing process. The dual-beam configuration enables more precise control of the heat input during laser brazing and is therefore expected to improve joint formation compared with the conventional single-beam process. In addition, previous studies on laser welding–brazing and dual-beam laser welding have reported that dual-beam configurations improve molten filler spreading, stabilize molten pool behavior, and suppress porosity compared with conventional single-beam processes (Ref 21, 22). Nevertheless, the mechanical performance and fracture behavior of joints produced by dual-beam laser brazing have not yet been sufficiently clarified.

Therefore, the present study investigates dissimilar laser brazing between an aluminum alloy and GA steel using a dual-beam laser system. Particular attention is paid to the relationship among wettability, blowhole formation, and tensile shear properties. Furthermore, the wetting and spreading behavior of molten filler metal is analyzed using computational simulations based on fluid dynamics theory considering a non-isothermal temperature field in order to clarify the fundamental mechanisms governing dual-beam laser brazing.

2. Experimental Procedure

The base metals used for the test specimens were 1.6-mm-thick A6061-T6 aluminum alloy sheets and 1.0-mm-thick SPCC-GA steel sheets. An Al–Si alloy flux-cored wire (AluS4Le) with a diameter of 1.2 mm was used as the filler material. The chemical compositions of these materials are summarized in Table 1. Laser brazing of the lap joint was performed using a fiber laser system, as shown in Fig. 1(a) and (b). Two laser brazing processes were employed: a single-beam process using one laser heat source and a dual-beam process using two laser heat sources. The specimens were mounted on a copper jig with an inclination angle of 15°, and brazing was performed. In the single-beam process, the laser beam was tilted by 10° in the brazing direction, and the filler wire was fed toward the center of the laser beam from the front side along the brazing direction. In the dual-beam process, two heat sources, namely a main laser and a preheating laser, were employed. The preheating laser was positioned 2.65 mm ahead of the main laser along the brazing direction and irradiated at an angle of 45°. The filler wire was fed toward the center of the main laser beam; however, unlike in the single-beam process, it was inclined by 40° in the horizontal direction due to the presence of the preheating laser ahead of the main laser.

To clarify the bonding characteristics of dual-beam laser brazing, experiments were conducted under various conditions by varying the main laser power and the preheating laser power, as summarized in Table 2. For comparison, single-beam laser brazing was also performed with the preheating laser power set to 0 W. The bonding range after brazing was evaluated based on the bead appearance. Cross-sectional observations of the brazed joints were carried out to measure the bead width, wetting angle, and intermetallic compound (IMC) thickness, as

Table 1 Chemical compositions of materials for laser brazing (mass %)

	Mg	Si	Mn	Fe	Cu	Cr	Zn	Ti	Al
A6061-T6	1.1	0.65	0.04	0.3	0.28	0.18	0.07	0.03	Bal.

	C	Mn	P	S	Fe
SPCC	0.05	0.18	0.015	0.003	Bal.

	Si	Fe	Cu	Mn	Mg	Zn	Al
Al-Si flux-cored wire	1.88	0.10	0.01	< 0.01	0.02	< 0.01	Bal.

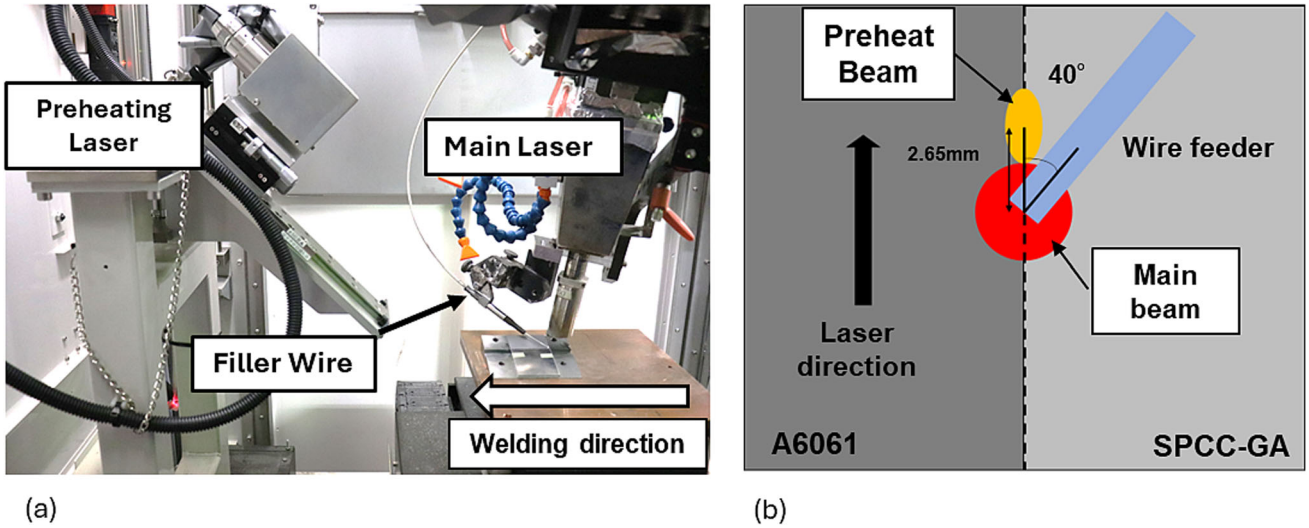

Fig. 1 (a) Photograph of the experimental setup for laser brazing and (b) schematic illustration of the laser brazing configuration

Table 2 Laser brazing conditions

	Main laser	Preheating laser
Laser equipment	6 kW fiber laser	500W fiber laser
Laser power, kW	0.7-2.1	0-400
Spot diameter, mm	3-4	1.6
Wire feeding speed, mm/s	20	
Brazing speed, mm/s	3.3	

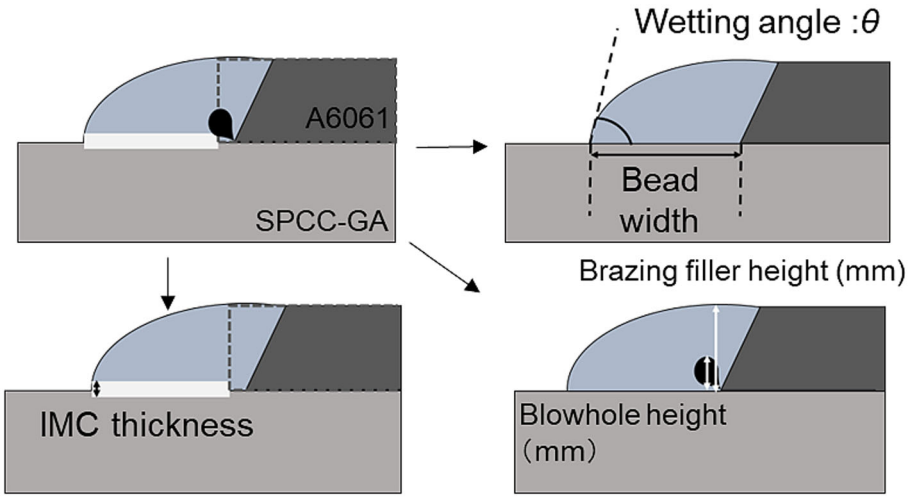

Fig. 2 Schematic illustration showing the definitions of weld toe angle, bead width, IMC thickness, and blowhole occupancy rate

illustrated in Fig. 2. In addition, the ratio of blowhole height to the filler metal height, defined as the blowhole occupancy rate, was determined. The mechanical properties of the brazed joints were evaluated at room temperature by tensile shear testing at a crosshead speed of 1.0 mm/min, as shown in Fig. 3. The joint strength (N/mm) was calculated by dividing the failure load by the specimen width. Tensile shear testing was conducted using five specimens for each condition ($N = 5$). The maximum and minimum values were excluded, and the average value of the remaining three specimens ($N = 3$) was used as the representative tensile shear strength. The scatter of the experimental results is indicated by error bars in the corresponding figures. Furthermore, under the optimum condition, dual-beam laser brazing was performed using 980DP-GA steel sheets. It should be noted that partial melting of the A6061 substrate locally occurred near the brazed interface under the present experi-

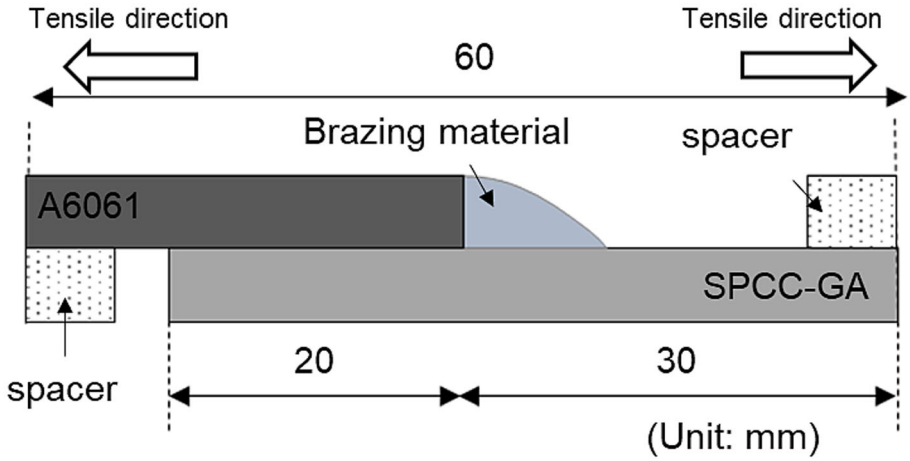

Fig. 3 Schematic illustration of the specimen used for the tensile test

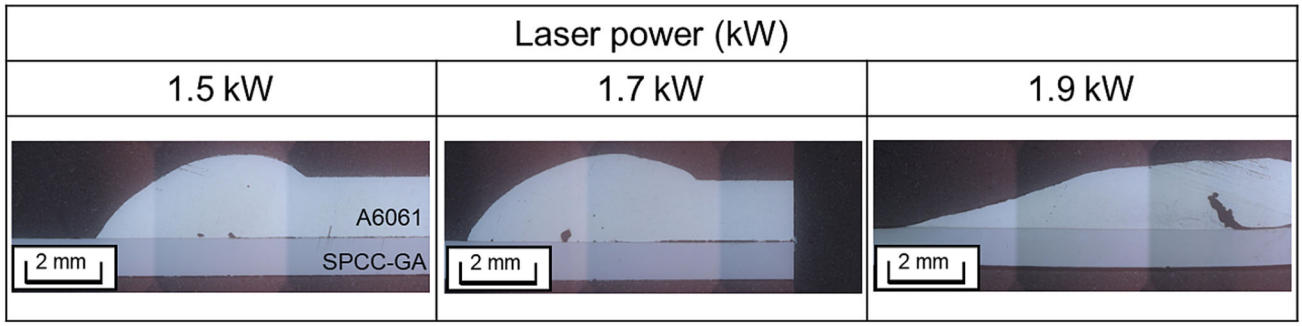

Fig. 4 Cross-sectional microstructures of joints produced by single-beam laser brazing

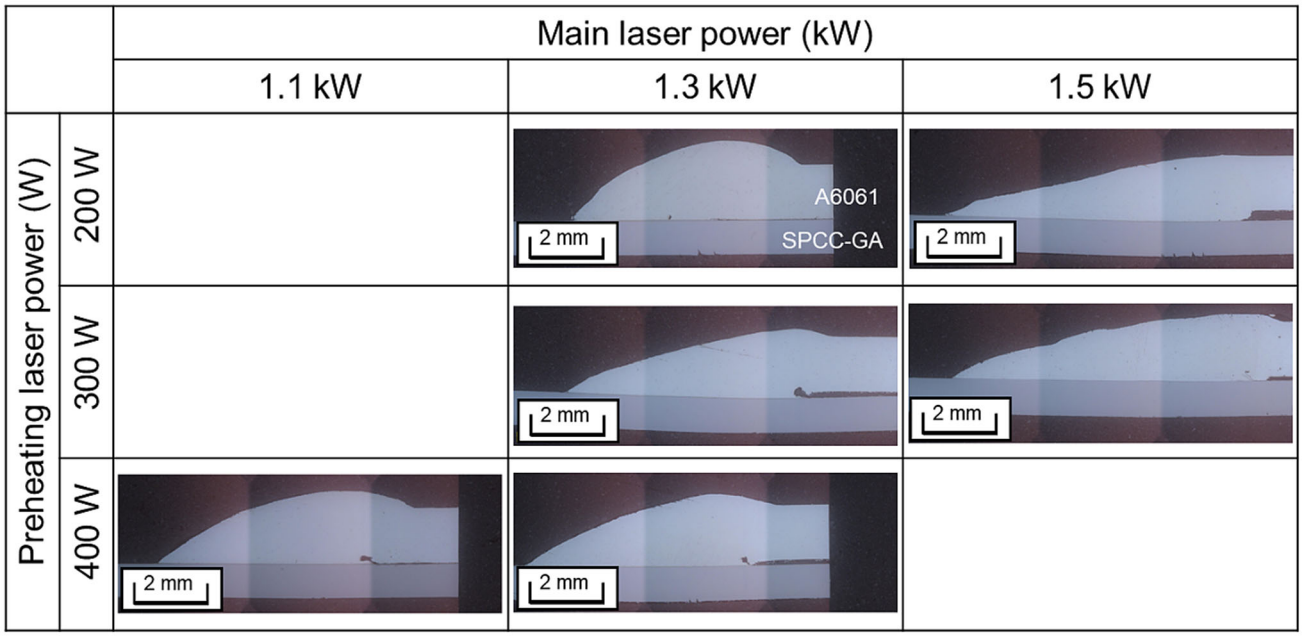

Fig. 5 Cross-sectional microstructures of joints produced by dual-beam laser brazing

mental conditions. Therefore, the present joining process may also be categorized as laser weld-brazing. However, since the primary joining mechanism was governed by molten filler metal spreading and interfacial reaction control, the term ''laser brazing'' is used throughout this study for simplicity.

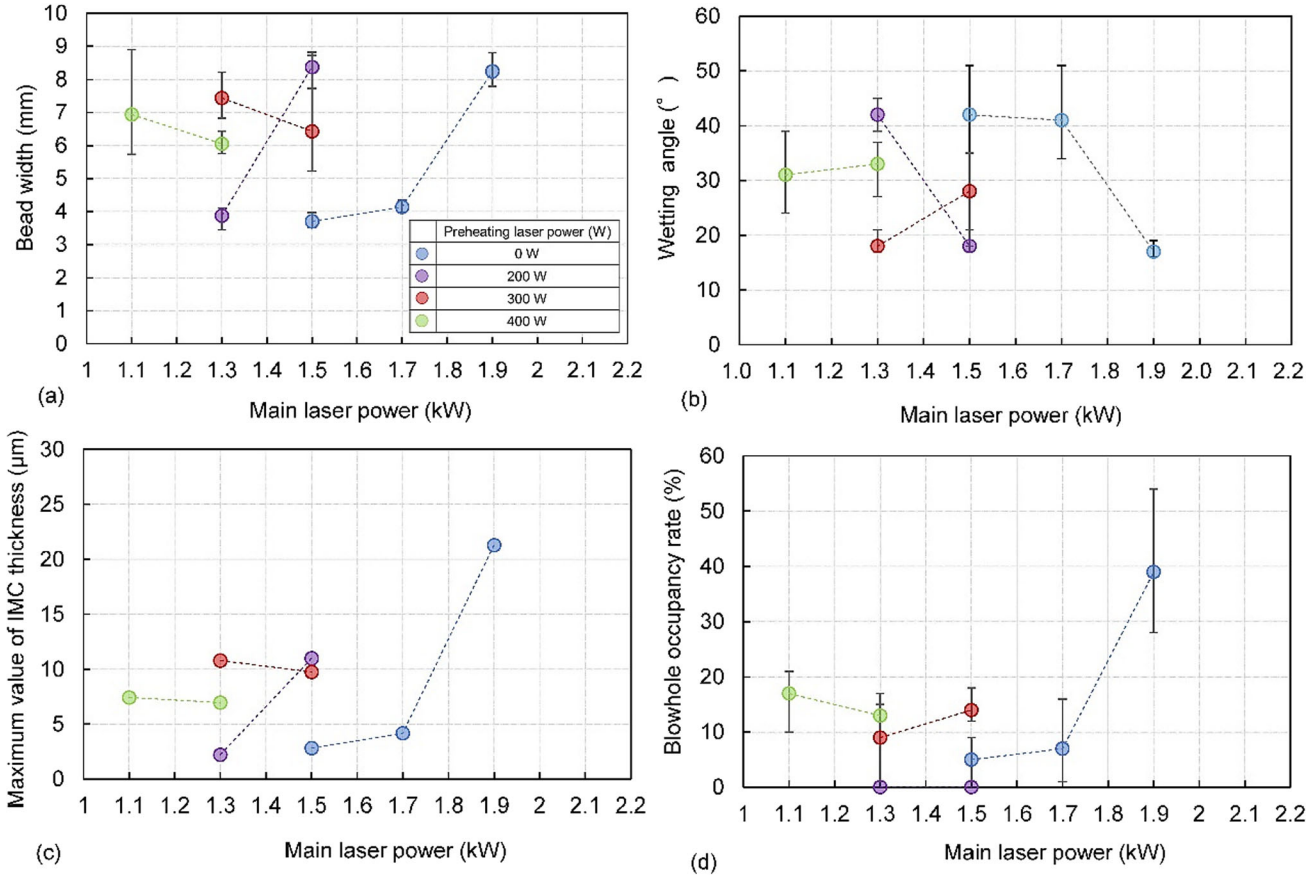

Fig. 6 Quantitative results showing the (a) bead width, (b) wetting angle, (c) maximum IMC thickness, and (d) blowhole occupancy rate as functions of laser power

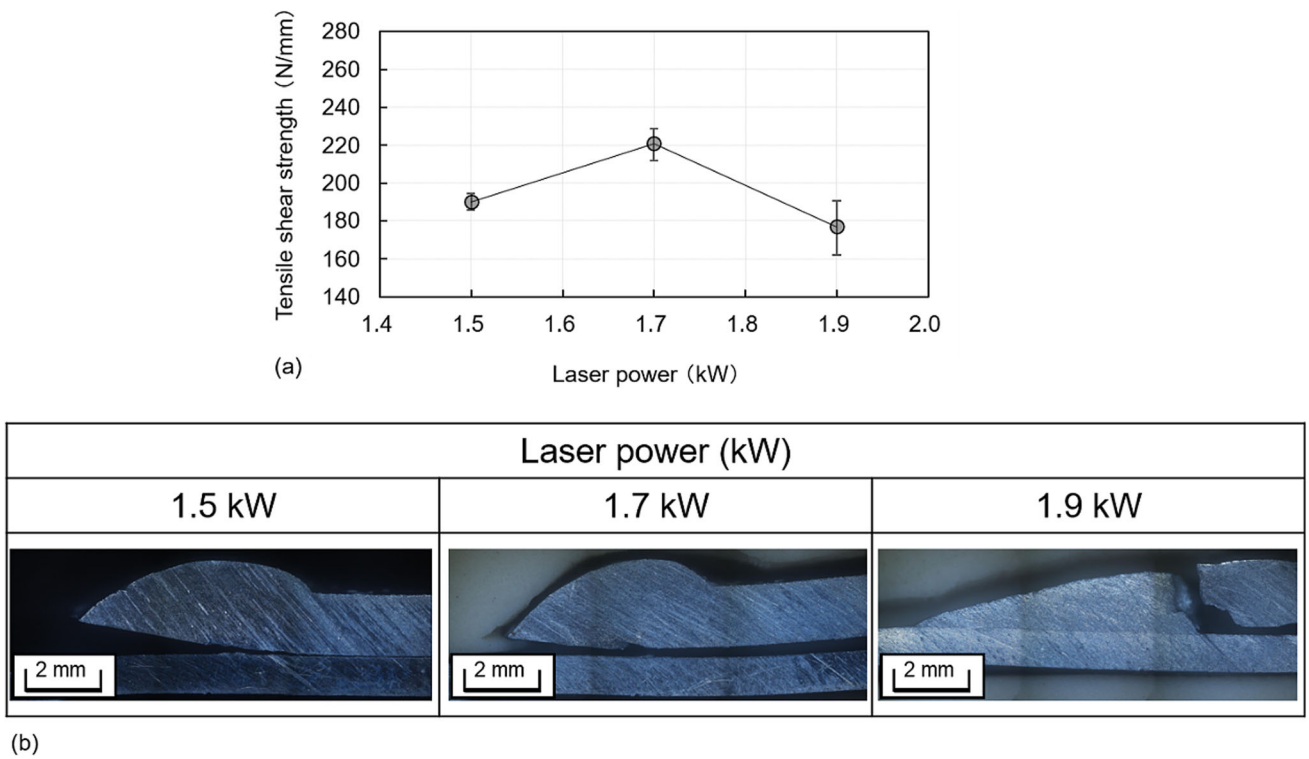

Fig. 7 (a) Tensile shear strength of A6061/SPCC-GA joints fabricated by single-beam laser brazing and (b) corresponding cross-sectional microstructures after fracture

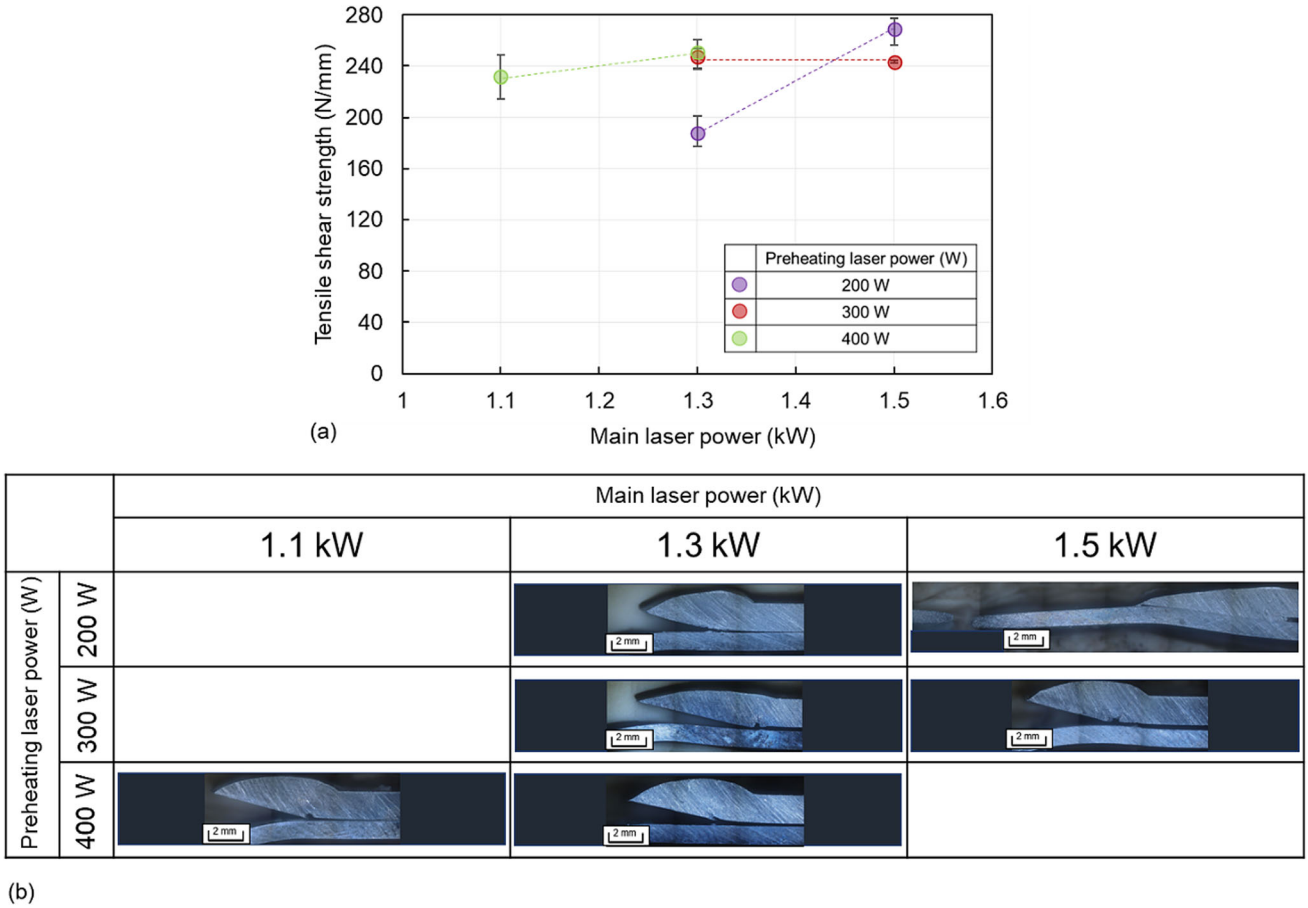

Fig. 8 (a) Tensile shear strength of A6061/SPCC-GA joints fabricated by dual-beam laser brazing and (b) corresponding cross-sectional microstructures after fracture

Table 3 Comparison of wettability, blowhole occupancy, IMC thickness, tensile shear strength, and fracture behavior between single-beam and dual-beam laser brazing under the respective optimum conditions

	Laser power, kW	Bead width, mm	Wetting angle, °	Maximum value of IMC thickness, μm	Blowhole occupancy rate, %	Tensile shear strength, N/mm	fracture mode
Single beam	1.7	4.1	41	4.2	7	221	Interface
Dual beam	0.2(pre-heating) 1.5(main)	8.4	18	11	0	269	SPCC-GA base metal

3. Results and Discussion

3.1 Effect of Laser Power on Microstructural Characteristics in Single-and Dual-Beam Laser Brazing of A6061/GA Steel

Figure 4 shows the cross-sectional microstructures obtained by single-beam laser brazing, while Fig. 5 shows those obtained by dual-beam laser brazing. In addition, Fig. 6 summarizes the bead width, wetting angle, maximum IMC thickness, and blowhole occupancy rate as functions of laser power for A6061/GA steel joints. In single-beam laser brazing, insufficient heat input at laser powers below 1.5 kW resulted in bonding defects such as incomplete melting of the filler wire. In contrast, excessive heat input at laser powers above 1.9 kW caused defects including irregular bead morphology and void formation. Within the laser power range of 1.5-1.9 kW, increasing the laser power increased the bead width and decreased the wetting angle, indicating improved wettability of the molten filler metal due to the increased heat input. However, at 1.9 kW, the blowhole occupancy rate increased markedly, accompanied by an increase in IMC thickness.

For the dual-beam laser brazing joints, the introduction of a preheating beam expanded the bonding window toward lower main laser powers. Moreover, under low heat-input conditions, the preheating beam suppressed blowhole formation and significantly improved wettability, as indicated by the bead width and wetting angle. In the dual-beam process, the

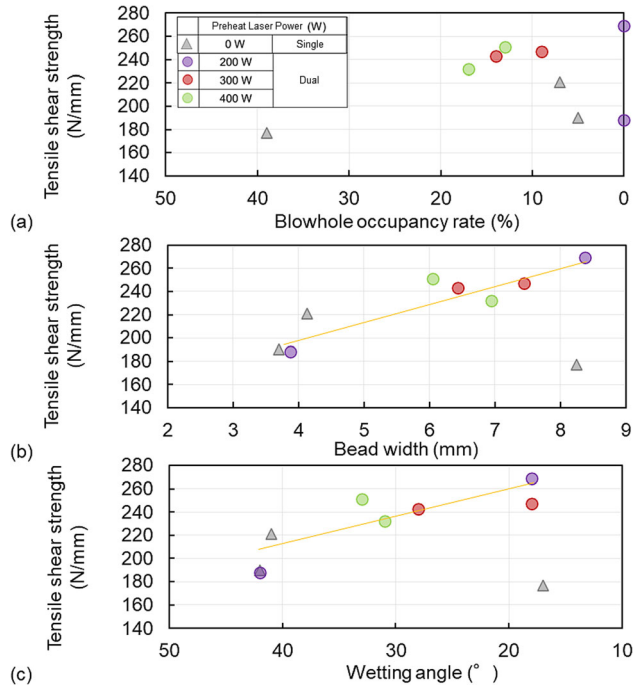

Fig. 9 Relationship between blowhole occupancy rate, bead width, wetting angle, and tensile shear strength

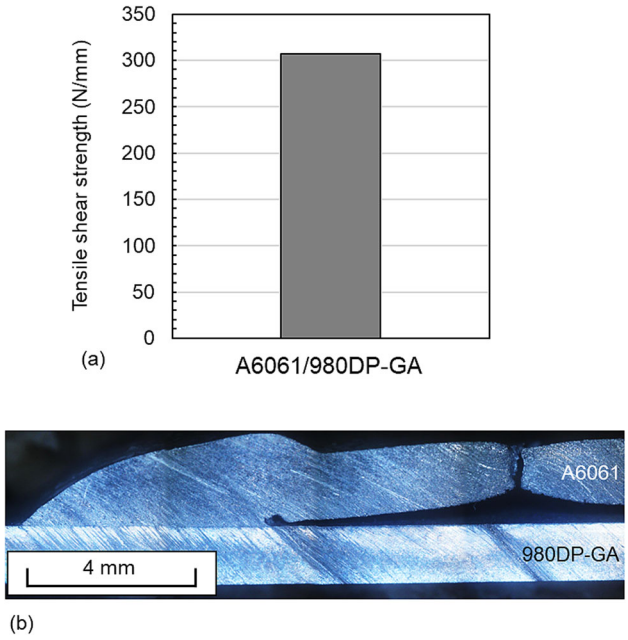

Fig. 10 (a) Tensile shear strength of A6061/980DP-GA joints fabricated by dual-beam laser brazing and (b) corresponding cross-sectional microstructures after fracture

maximum IMC thickness remained approximately 10 μm and did not increase significantly with increasing main laser power up to 1.5 kW. Although detailed phase identification of the IMC layer was not conducted in the present study, previous studies on Al/steel dissimilar laser brazing have reported the formation of $FeAl_3$ at the interface (Ref 19). These phases are generally brittle and deteriorate joint properties when excessively thick layers are formed. In the present study, the IMC thickness remained approximately 10 μm even in the dual-beam process, which contributed to the improved joint strength. These results demonstrate that dual-beam laser brazing simultaneously improves wetting behavior and suppresses blowhole formation. Furthermore, the results suggest that improved wettability and reduced blowhole formation strongly influence the mechanical performance of the joints. Therefore, tensile shear properties were subsequently investigated.

3.2 Effect of Single-and Dual-Beam Laser Brazing on Joint Strength and Fracture Behavior of A6061/GA Steel Joints

To evaluate the joint strength of dissimilar laser-brazed A6061/SPCC-GA joints, tensile shear tests were conducted. The results for single-beam laser brazing are shown in Fig. 7(a), and the corresponding cross-sectional microstructures after fracture are shown in Fig. 7(b). The maximum fracture strength was obtained at a laser power of 1.7 kW, reaching 221 N/mm, corresponding to approximately 82% of the base metal strength of SPCC (270 N/mm). In contrast, the minimum fracture strength was obtained at a laser power of 1.9 kW, with a value of 177 N/mm. Fracture occurred along the interface at laser powers of 1.5 and 1.7 kW, whereas at 1.9 kW, fracture occurred within the filler metal and was initiated from blowholes. For the dual-beam laser brazing joints, tensile shear tests were also conducted. The results are shown in Fig. 8(a), and the corresponding cross-sectional microstructures after fracture are shown in Fig. 8(b). The maximum fracture strength was obtained under a main laser power of 1.5 kW and a preheating laser power of 200 W, reaching 269 N/mm, corresponding to approximately 99% of the base metal strength of SPCC. Notably, fracture occurred in the SPCC base metal under this condition, indicating that the joint strength was comparable to that of the base metal and demonstrating the superior joint performance achieved by dual-beam laser brazing. To clearly compare the effects of the single-beam and dual-beam laser brazing processes, the results obtained under the respective optimum conditions are summarized in Table 3. The dual-beam process exhibited improved wettability, lower blowhole occupancy, and higher tensile shear strength than the conventional single-beam process, although the IMC thickness slightly increased.

To clarify how the microstructure after laser brazing influences tensile shear strength, as well as the effect of the dual-beam process, the relationships among blowhole occupancy rate, bead width, wetting angle, and tensile shear strength were analyzed. The results are summarized in Fig. 9. No significant difference in IMC thickness was observed between the dual-beam and single-beam laser brazing processes at main laser powers of 1.5 kW or lower, where the blowhole occupancy rate remained low. Therefore, IMCs are not considered to be the dominant factor governing fracture behavior in the present study. For the blowhole occupancy rate and wetting angle, the graphs were arranged such that the minimum values are located on the right-hand side of the axes. Although some blowholes were observed even in the dual-beam laser brazing joints, no fracture within the filler metal occurred when the blowhole occupancy rate was below 20%. This result indicates that blowholes formed under these conditions had a negligible effect on fracture behavior. Furthermore, the bead width was larger and the wetting angle was lower in the dual-beam process than in the single-beam

Table 4 Material constants used for computer simulation

Liquid	Brazing material, Alu S4Le	Base Material, A6061
Density, kg/m^3	2702	2705
Viscosity, kg/m/s	$-8 \times 10^{-4}\ln(T) + 0.0066$	0.00115
specific heat, J/kg/C	1180	870
Thermal conductivity, W/m/C	0.0354 T + 67.474	195
Liquidus Temperature, °C	662	642
Solid phase temperature, °C	575	600
latent heat, J/kg	3.97×10^5	3.36×10^5
Surface tension coefficient, kg/s^3	974-0.2 T	871
Solid		**Base Material (GA-steel)**
Thermal conductivity, W/m/C		80.2
Density and heat capacity, kg/m/s^2/C		3.46e + 6
Contact angle, °		0.0067 T + 25.6667 (measurements)

process. These results indicate that the dual-beam configuration improves the wettability of the molten filler metal, resulting in enhanced joint strength. Based on these findings, dual-beam laser brazing enables the fabrication of high-quality joints achieving base metal fracture and is therefore superior to the conventional single-beam process.

The optimum condition identified in this study (preheating laser power: 200 W; main laser power: 1.5 kW) was also applied to A6061/980DP-GA dissimilar laser-brazed joints, followed by tensile shear testing. The tensile shear test results are shown in Fig. 10(a). The joint exhibited a tensile shear strength of 307 N/mm, corresponding to approximately 97% of the base metal strength of A6061 (315 N/mm). The cross-sectional microstructure after fracture is shown in Fig. 10(b), where fracture occurred in the A6061 base metal. This base metal fracture indicates that the joint strength exceeded that of both the interface and the filler metal, demonstrating that a highly reliable and high-quality joint was successfully achieved.

These results further suggest that the optimized process parameters identified for A6061/SPCC-GA joints can also be applied to other steel grades, enabling the fabrication of high-performance dissimilar joints. The suppression of blowhole formation in the dual-beam process is considered to be closely related to the interfacial thermal history and molten filler metal flow behavior. In the single-beam process, localized rapid heating promotes abrupt melting and vaporization of the Zn-rich coating, resulting in unstable molten pool behavior and entrapment of Zn vapor. In contrast, the preheating beam gradually increases the interface temperature before molten filler inflow, reducing sudden Zn vapor generation and promoting stable molten filler spreading.

3.3 Numerical Modeling of Wetting and Spreading Behavior in Single-and Dual-Beam Laser Brazing

A numerical simulation framework was developed to predict the wetting and spreading behavior of molten filler metal in dissimilar laser brazing and to elucidate the underlying wetting dynamics. Based on previous studies (Ref 20), three-dimensional models for single- and dual-beam laser brazing were constructed. The material properties used in the simulations are summarized in Table 4. The filler metal and the A6061 substrate were treated as liquid phases, whereas the SPCC-GA substrate was treated as a solid phase. The properties of the filler metal were approximated using those of pure aluminum, and temperature-dependent properties were assigned to viscosity, thermal conductivity, and surface tension. The A6061 substrate was also described using temperature-dependent thermophysical properties. For the SPCC-GA substrate, selected properties were approximated using those of pure iron. In addition, temperature-dependent wettability parameters were introduced to account for the wetting behavior of the galvanized coating. The validity of the developed model was assessed by comparing the simulation results with the corresponding experimental observations. In the present simulation, several thermophysical properties that were unavailable for the AluS4Le filler wire and SPCC-GA steel sheets were approximated using pure aluminum and pure iron properties. However, the contact angle used for the wettability analysis was experimentally measured using the actual filler metal and SPCC-GA steel sheets. Therefore, the experimentally observed interfacial wettability behavior was directly reflected in the analytical model.

The validity of the developed model was assessed by comparing the simulation results with the corresponding experimental observations. In the present simulation, several thermophysical properties that were unavailable for the AluS4Le filler wire and SPCC-GA steel sheets were approximated using pure aluminum and pure iron properties. However, the contact angle used for the wettability analysis was experimentally measured using the actual filler metal and SPCC-GA steel sheets. Therefore, the experimentally observed interfacial wettability behavior was directly reflected in the analytical model. The validity of the analytical model for single-beam laser brazing was first evaluated. Simulations were performed at main laser powers of 1.5 and 1.7 kW, and the bead width and wetting angle were measured from the cross-sectional profiles obtained from the simulations. The results are shown in Fig. 11. Increasing laser power improved wetting behavior, which is consistent with the experimental observations. The validity of the analytical model was subsequently evaluated for dual-beam laser brazing. The results are shown in Fig. 12. Simulations were conducted by varying the preheating laser power while maintaining the main laser power at 1.3 kW. Similar to single-beam brazing, improved wetting behavior was observed with increasing laser power, in agreement with the

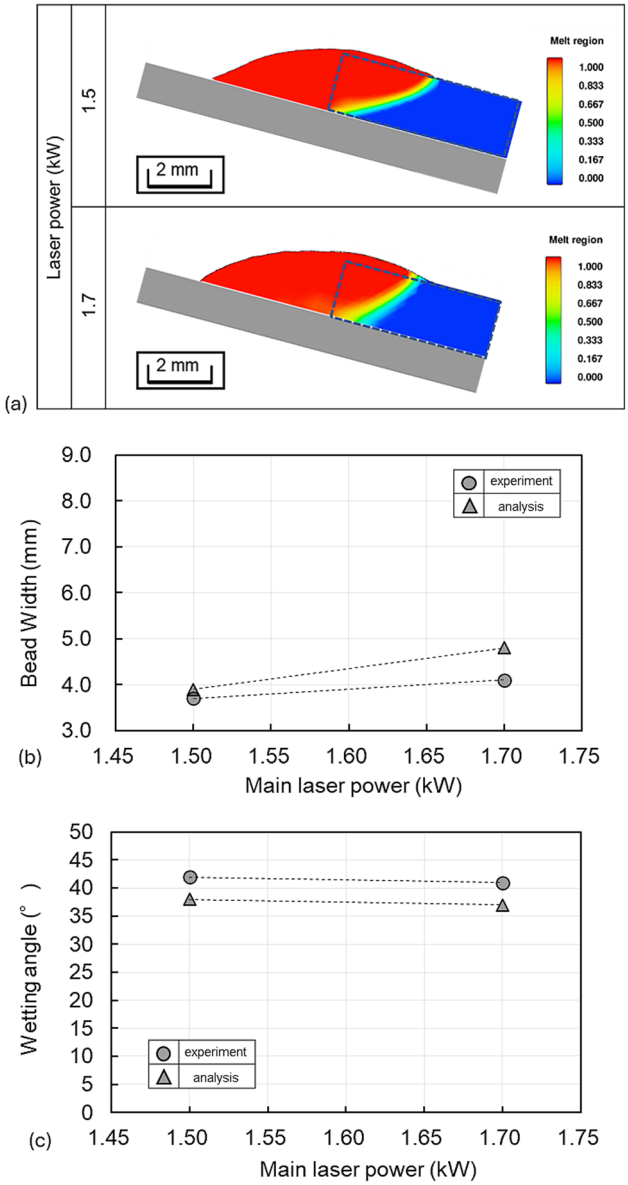

Fig. 11 (a) Simulated microstructures and comparison of (b) bead width and (c) wetting angle with experimental results as a function of laser power, using the single-beam laser model

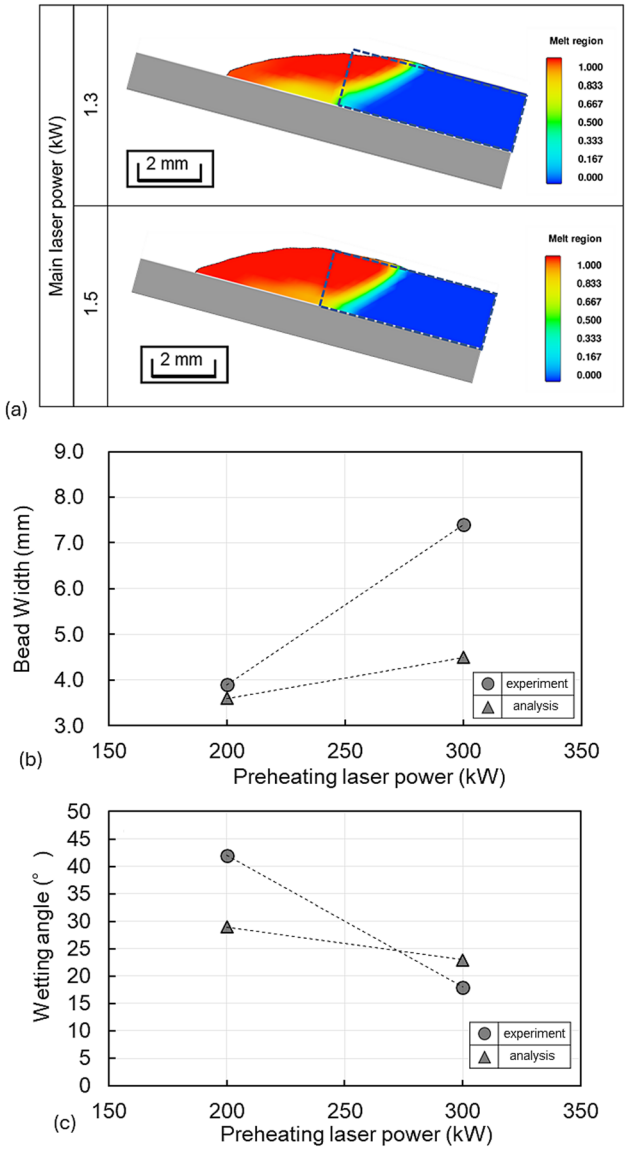

Fig. 12 (a) Simulated microstructures and comparison of (b) bead width and (c) wetting angle with experimental results as a function of laser power, using the dual-beam laser model

experimental results. These results indicate that the present model can qualitatively predict the spreading behavior of molten filler metal. Therefore, a predictive model for the wetting and spreading behavior of molten filler metal during laser brazing was successfully established. The developed numerical model was subsequently applied to investigate how the experimentally observed improvement in wettability under dual-beam conditions is related to molten filler spreading behavior and interface temperature distribution. Next, the models were applied to investigate the wetting and spreading behavior at a fixed main laser power of 1.5 kW for both the single-beam and dual-beam configurations (with a 200 W preheating beam), as shown in Fig. 13. Comparison under the same main laser power indicates that the addition of a preheating beam in the dual-beam configuration improves wettability.

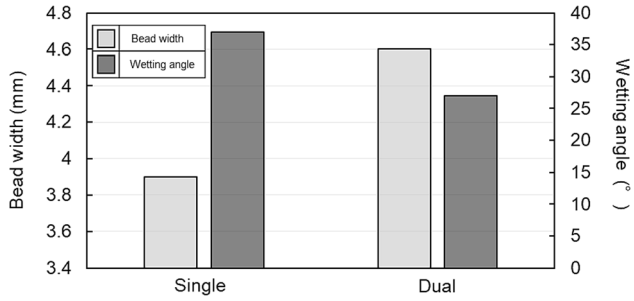

Fig. 13 Wetting and spreading of filler metal at a main laser power of 1.5 kW for (a) single-beam and (b) dual-beam configurations (200 W preheating)

To clarify the wetting and spreading behavior in single-beam and dual-beam laser brazing, the temporal evolution of filler metal spreading after brazing initiation was evaluated. The

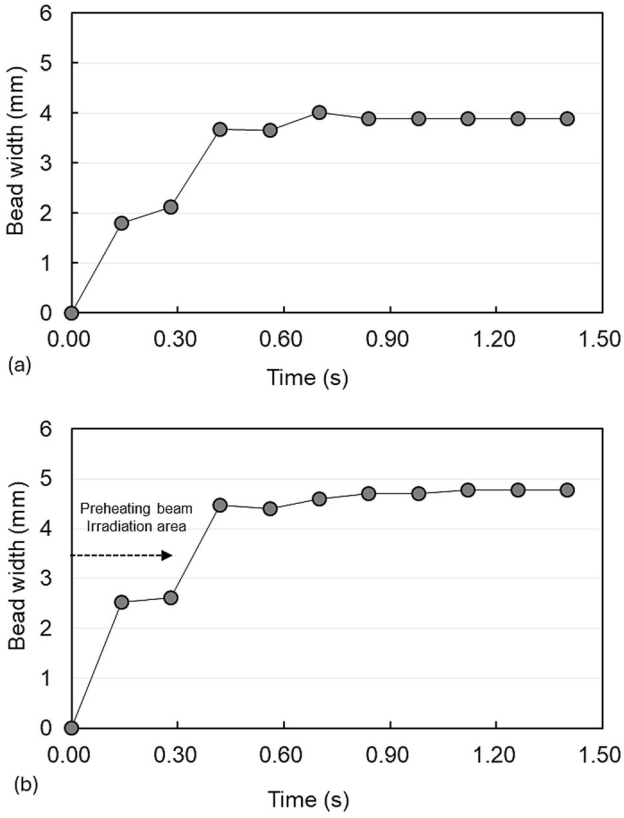

Fig. 14 Temporal evolution of filler metal spreading and the corresponding time-dependent bead width for (a) single-beam and (b) dual-beam laser brazing configurations

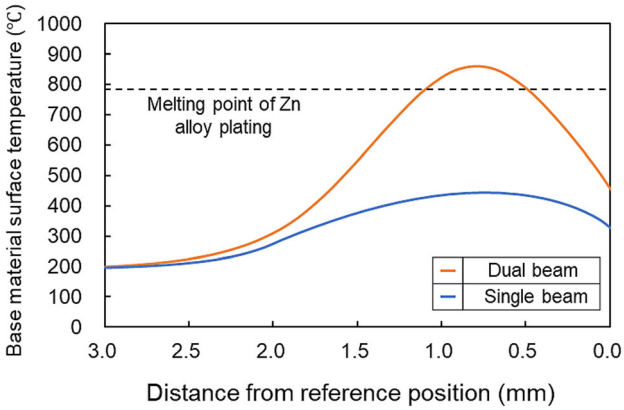

Fig. 15 SPCC-GA interface temperature just before filler metal inflow for single- and dual-beam configurations

time-dependent bead width is shown in Fig. 14. The results indicate that the primary difference between the single-beam and dual-beam configurations occurs during the initial stage of wetting and spreading. In the single-beam case (Fig. 14a), immediately after brazing initiation (< 0.3 s), the initially melted filler metal flowed into the joint region. Once the filler wire entered the laser irradiation zone and became fully molten, rapid wetting and spreading occurred. The spreading behavior then gradually stabilized, and the bead width reached an approximately constant value after passing through the laser irradiation zone. In contrast, in the dual-beam configuration (Fig. 14b), significant wetting and spreading were observed immediately after brazing initiation (< 0.3 s) because of preheating beam irradiation prior to main beam exposure. Subsequent irradiation by the main laser beam further enhanced spreading, which eventually reached a steady-state value. Overall, the wetting and spreading behavior in the dual-beam configuration was more pronounced than that in the single-beam configuration. These findings suggest that the key difference in wetting and spreading behavior between the two configurations originates from the initial spreading of molten filler metal into the joint region.

To clarify the enhanced wetting and spreading observed immediately after brazing initiation in the dual-beam configuration, the SPCC-GA interface temperature immediately before molten filler inflow was analyzed. The results are shown in Fig. 15, where 0 mm corresponds to the position of main laser irradiation, and the positive direction represents the molten filler spreading direction. As shown in Fig. 15, the interface temperature in the dual-beam case was substantially higher than that in the single-beam case and exceeded the melting point of the GA coating, indicating that the coating had already melted because of preheating. These simulation results suggest that the enhanced wetting and spreading observed in the dual-beam process are primarily attributable to preheating-induced melting of the GA coating prior to molten filler inflow.

4. Conclusions

Dual-beam laser brazing of dissimilar A6061/SPCC-GA joints was performed, and the wetting and spreading behavior of molten filler metal was investigated through both experimental and numerical analyses to elucidate the underlying mechanisms.

1. Dual-beam laser brazing simultaneously improved wetting behavior, suppressed blowhole formation, and maintained IMC thickness.
2. The optimum condition identified in this study (preheating laser power: 200 W; main laser power: 1.5 kW) resulted in base metal fracture for both A6061/SPCC-GA and A6061/980DP-GA joints, demonstrating the superior joint performance achieved by dual-beam laser brazing.
3. The simulation results showed that increasing laser power increased the wetting width and decreased the wetting angle, consistent with the experimental results, indicating that the wetting and spreading behavior can be qualitatively predicted.
4. The enhanced wetting and spreading observed in the dual-beam process are primarily attributable to preheating-induced melting of the GA coating prior to molten filler inflow.

Acknowledgments

This study was supported by a project commissioned by the New Energy and Industrial Technology Development Organization (NEDO). The authors also gratefully acknowledge partial financial support from the Light Metal Educational Foundation, Inc.

Funding

Open Access funding provided by The University of Osaka.

Open Access

This article is licensed under a Creative Commons Attribution 4.0 International License, which permits use, sharing, adaptation, distribution and reproduction in any medium or format, as long as you give appropriate credit to the original author(s) and the source, provide a link to the Creative Commons licence, and indicate if changes were made. The images or other third party material in this article are included in the article's Creative Commons licence, unless indicated otherwise in a credit line to the material. If material is not included in the article's Creative Commons licence and your intended use is not permitted by statutory regulation or exceeds the permitted use, you will need to obtain permission directly from the copyright holder. To view a copy of this licence, visit http://creativecommons.org/licenses/by/4.0/.

References

1. W.S. Miller, L. Zhuang, J. Bottema, A. Wittebrood, P. De Smet, A. Haszler, and A.J.M.S. Vieregge, Recent Development in Aluminium Alloys for the Automotive Industry, *Mater. Sci. Eng. A*, 2000, **280**(1), p 37–49. https://doi.org/10.1016/S0921-5093(99)00653-X
2. G.S. Cole and A.M. Sherman, Light Weight Materials for Automotive Applications, *Mater Charact*, 1995, **35**(1), p 3–9. https://doi.org/10.1016/1044-5803(95)00063-1
3. Y. Yang, Z. Luo, Y. Zhang, and J. Su, Dissimilar Welding of Aluminium to Steel: A Review, *J. Manuf. Process.*, 2024, **110**, p 376–397. https://doi.org/10.1016/j.jmapro.2023.12.060
4. G. Meschut, V. Janzen, and T. Olfermann, Innovative and Highly Productive Joining Technologies for Multi-material Lightweight Car Body Structures, *J. Mater. Eng. Perform.*, 2014, **23**, p 1515–1523. https://doi.org/10.1007/s11665-014-0962-3
5. H. Springer, A. Kostka, E.J. Payton, D. Raabe, A. Kaysser-Pyzalla, and G. Eggeler, On the Formation and Growth of Intermetallic Phases in Steel–Aluminum Joints, *Acta Mater.*, 2011, **59**(4), p 1586–1600. https://doi.org/10.1016/j.actamat.2010.11.023
6. R.S. Mishra and Z.Y. Ma, Friction Stir Welding and Processing, *Mater. Sci. Eng. R*, 2005, **50**(1–2), p 1–78. https://doi.org/10.1016/j.mser.2005.07.001
7. T. Ogura, Y. Saito, T. Nishida, H. Nishida, S. Yoshikawa, M. Fujimoto, and A. Hirose, Partitioning Evaluation of Mechanical Properties and the Interfacial Microstructure in a Friction Stir Welded Aluminum Alloy/Stainless Steel Lap Joint, *Scr. Mater.*, 2012, **66**(8), p 531–534. https://doi.org/10.1016/j.scriptamat.2011.12.035
8. T. Ogura, Y. Tanaka, K. Shimizu, and A. Hirose, Evaluation of Joint Properties and Theoretical Analysis of Dissimilar Friction Welding Between Al-11%Zn-3%Mg-1.4%Cu Alloy and SUS304 Stainless Steel, *Mater. Trans.*, 2025, **66**(12), p 1577–1584. https://doi.org/10.2320/matertrans.MT-L2025010
9. Z. Zhang, H. Wang, J. Liu, Y. Zhao, X. Chen, Y. Li, and J. Wang, Interfacial Microstructure and Mechanical Properties of Al/Steel Joints Fabricated via Thermo-Compensated Resistance Brazing Welding with Cold Spray Zn Interlayer, *J. Mater. Res. Technol.*, 2023, **24**, p 5094–5107. https://doi.org/10.1016/j.jmrt.2023.04.081
10. J. Yang, J.P. Oliveira, Y. Li, C. Tan, C. Gao, Y. Zhao, and Z. Yu, Laser Techniques for Dissimilar Joining of Aluminum Alloys to Steels: A Critical Review, *J. Mater. Process. Technol.*, 2022, **301**, p 117443. https://doi.org/10.1016/j.jmatprotec.2021.117443
11. T. Ogura, S. Netsu, T. Yokochi, and K. Saida, Microstructure and Mechanical Properties in Laser Brazing of A5052/AZ31 Dissimilar Alloys, *Weld. World*, 2016, **60**, p 1047–1054. https://doi.org/10.1007/s40194-016-0363-3
12. T. Ogura, S. Netsu, K. Ike, and K. Saida, Effects of Titanium Interlayer on Dissimilar Joining Between Aluminum Alloy and Magnesium Alloy Using LASER Brazing, *Q. J. Jpn. Weld. Soc.*, 2018, **36**(4), p 247–252. https://doi.org/10.2207/qjjws.36.247
13. A.R. Marder, The Metallurgy of Zinc-Coated Steel, *Prog. Mater. Sci.*, 2000, **45**(3), p 191–271. https://doi.org/10.1016/S0079-6425(98)00006-1
14. D. Yang, K. Wang, H. Zhou, X. Zhang, B. Zhang, B. Lu, and F. Wang, Microstructure and Properties of Galvannealed Coatings at Different Galvannealed Time, *Mater. Lett.*, 2023, **345**, p 134489. https://doi.org/10.1016/j.matlet.2023.134489
15. T. Wakisaka and T. Suzuki, Laser Brazing of Aluminum Alloy and Galvannealed Steel with Zn–Si Filler Metal, *Q. J. Jpn. Weld. Soc.*, 2012, **30**(3), p 274–279. https://doi.org/10.2207/qjjws.30.274
16. L. Jia, S. Jiang, Y. Shi, C. Ni, J. Chen, and G. Huang, Effects of Zinc on the Laser Welding of an Aluminum Alloy and Galvanized Steel, *J. Mater. Process. Technol.*, 2015, **224**, p 49–59. https://doi.org/10.1016/j.jmatprotec.2015.04.017
17. H. Dong, S. Chen, Y. Song, X. Guo, X. Zhang, and Z. Sun, Refilled Friction Stir Spot Welding of Aluminum Alloy to Galvanized Steel Sheets, *Mater. Des.*, 2016, **107**, p 529–537. https://doi.org/10.1016/j.matdes.2016.07.052
18. G. Sierra, P. Peyre, F. Deschaux Beaume, D. Stuart, and G. Fras, Galvanised Steel to Aluminium Joining by Laser and GTAW Processes, *Mater Charact*, 2008, **59**(12), p 1705–1715. https://doi.org/10.1016/j.matchar.2008.03.016
19. T. Ogura, R. Wakazono, S. Yamashita, and K. Saida, Dissimilar Laser Brazing of Aluminum Alloy and Galvannealed Steel and Defect Control Using Interlayer, *Weld. World*, 2020, **64**(4), p 697–706. https://doi.org/10.1007/s40194-020-00858-7
20. S. Yamashita, T. Ogura, H. Hirata, and K. Saida, Coupled Analysis of Bead Shape and Intermetallic Compound Thickness in Dissimilar Laser Brazing of High-Strength Steel and Aluminum Alloy, *Q. J. Jpn. Weld. Soc.*, 2024, **42**(2), p 97–104. https://doi.org/10.2207/qjjws.42.97
21. H. Xia, S. Li, L. Li, G. Tan, Y. Chen, and J. Wang, Effect of Laser Beam Models on Laser Welding–Brazing Al to Steel, *Opt. Laser Technol.*, 2020, **122**, p 105845. https://doi.org/10.1016/j.optlastec.2019.105845
22. X. Xie, W. Huang, J. Zhou, and J. Long, Study on the Molten Pool Behavior and Porosity Formation Mechanism in Dual-Beam Laser Welding of Aluminum Alloy, *J. Laser Appl.*, 2022, **34**(2), p 022007. https://doi.org/10.2351/7.0000630

Publisher's Note Springer Nature remains neutral with regard to jurisdictional claims in published maps and institutional affiliations.